

Fast dynamics of H₂O in hydrous aluminosilicate glasses studied with quasielastic neutron scattering

Sylvio Indris* and Paul Heitjans[†]*Institut für Physikalische Chemie und Elektrochemie, Universität Hannover, Callinstraße 3-3A, D-30167 Hannover, Germany*

Harald Behrens

Institut für Mineralogie, Universität Hannover, Callinstraße 3, D-30167 Hannover, Germany

Reiner Zorn

Institut für Festkörperforschung, Forschungszentrum Jülich GmbH, D-52425 Jülich, Germany

Bernhard Frick

Institut Laue-Langevin, 6 rue Jules Horowitz, F-38042 Grenoble, Cedex 9, France

(Received 14 July 2004; published 25 February 2005)

We studied the dynamics of dissolved water in aluminosilicate glasses with the compositions NaAlSi₃O₈·0.3H₂O, NaAlSi₃O₈·1.3H₂O and Ca_{0.5}AlSi₃O₈·1.3H₂O using quasielastic neutron scattering. As shown by near-infrared spectroscopy on these samples, H₂O molecules are the predominant hydrous species in the water-rich glasses whereas OH groups bound to tetrahedrally coordinated cations are predominant at low water contents. Backscattering and time-of-flight methods were combined to investigate motional correlation times in the range between 0.2 ps and 2 ns. For the water-rich glasses an elastic scan between 2 K and 420 K shows that the dynamical processes set in at lower temperatures in the Ca-bearing glass than in the Na-bearing glass. This is corroborated by the broadening of the inelastic spectra $S(Q, \omega)$. The shape of the scattering function $S(Q, t)$ suggests a distribution of activation barriers for the motion of hydrous species in the disordered structure of the glass. The distribution is narrower and the average activation energy is smaller in the Ca-bearing glass than in the Na-bearing glass. No indication for dynamics of hydrous species was found at temperatures up to 520 K in the water-poor glass NaAlSi₃O₈·0.3H₂O containing dissolved water mainly in the form of OH groups. It is concluded that H₂O molecules are the dynamic species in the above-mentioned time regime in the water-rich glasses. The dynamic process is probably a rotation of H₂O molecules around their bisector axis.

DOI: 10.1103/PhysRevB.71.064205

PACS number(s): 61.12.-q, 61.43.Fs, 66.30.-h, 93.85.+q

I. INTRODUCTION

Knowledge of dynamic processes of hydrous species in silicate glasses is important in geosciences and materials science, e.g., for understanding and modeling of processes during volcanic eruptions and corrosion of glass. Glasses produced by quenching silicate melts at ambient pressure contain usually not more than a few hundreds to thousands of ppm by weight of H₂O. Nevertheless, these small quantities of dissolved water can have large effects on physical and chemical properties of the glasses, e.g., lowering the glass transition temperature by several tens to hundreds of kelvin¹⁻³ and decreasing strongly the optical transmittance in the mid-infrared.⁴ Larger amounts of dissolved H₂O of up to 8 wt. % are found in natural glasses of volcanic origin, either in small quantities as glass inclusions in minerals⁵ or as extended rocks such as pitchstone.⁶ Water-rich layers containing sometimes more than 10 wt. % H₂O can be formed by corrosion of glasses. Such hydration layers have been used for dating obsidian artifacts.⁷ In the laboratory up to 20 wt. % H₂O can be incorporated in silicate glasses by fusion of glass powder and H₂O at high pressure.^{8,9}

As shown by near-infrared (NIR) and nuclear magnetic resonance (NMR) spectroscopy, water dissolves in silicate

glasses and melts in the form of at least two different species, OH groups and H₂O molecules.^{4,8,10-13} Figure 1 shows a sketch of the structure of hydrous alkali and alkaline earth aluminosilicate glasses. In these glasses aluminium is incorporated on tetrahedral sites with its charge being compensated by Na⁺ or Ca²⁺. SiO₄ and AlO₄ tetrahedra form a completely polymerized three dimensional network. Introducing water as OH groups leads to disruption of oxygen bridges and thus to a softening of the network while molecular water leaves the network unchanged. For low water contents OH groups are the dominant hydrous species in glasses, but with increasing water content H₂O molecules become more abundant whereas the OH concentration reaches a constant level.^{4,8,14,15}

Information on the dynamics of hydrous species in silicate glasses is available for elevated temperatures from studies on water diffusion, electrical conductivity, internal friction and water speciation. Much less is known about motions of such species at low temperatures. NMR observations indicate that rotation of H₂O molecules around their bisector axis can be activated in alkali aluminosilicate glasses already at temperatures around 140 K but details of this motional process are unknown.^{12,13,16,17} In this paper we have investigated the dynamics of hydrous species in silicate glasses at temperatures

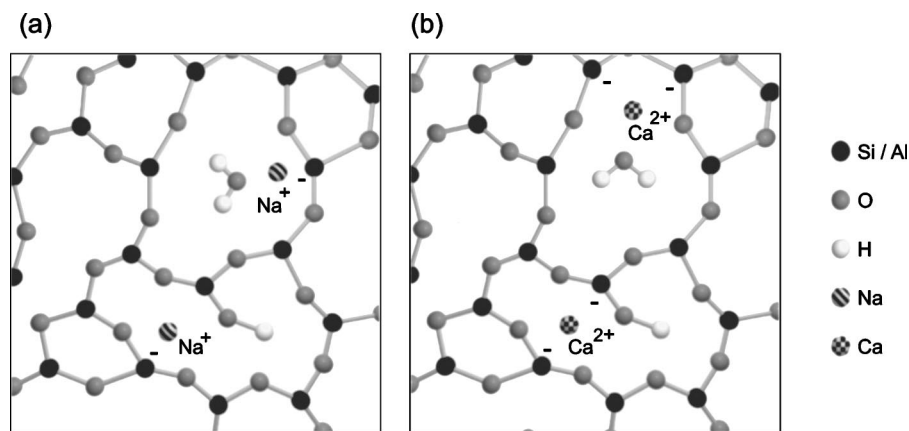


FIG. 1. Sketch of the structure of (a) an alkali and (b) an alkaline-earth aluminosilicate glass containing water in molecular form and as OH groups. The excess charge of tetrahedrally coordinated aluminium (AlO_4^- , marked with a minus sign) is balanced by alkali and alkaline-earth ions, respectively. For the sake of clarity, in this two-dimensional plot the Si as well as the Al atoms are drawn as threefold coordinated.

ranging from 2 K to 423 K using incoherent quasielastic neutron scattering. Combining neutron time-of-flight and backscattering spectroscopy, motional correlation times³⁷ in the range from 0.2 ps to 2 ns are covered. For a detailed description of these methods see, e.g., Refs. 18 and 19. Measurements were performed on two hydrated glasses with the anhydrous compositions $\text{NaAlSi}_3\text{O}_8$ and $\text{Ca}_{0.5}\text{AlSi}_3\text{O}_8$ which show a large difference in bulk water diffusivity D_{water} . At 1 wt. % water content (corresponding to the compositions $\text{NaAlSi}_3\text{O}_8 \cdot 0.15\text{H}_2\text{O}$ and $\text{Ca}_{0.5}\text{AlSi}_3\text{O}_8 \cdot 0.15\text{H}_2\text{O}$, respectively) and $T=870$ K, D_{water} is about two orders of magnitude greater in the Na-bearing than in the Ca-bearing glass ($8.9 \times 10^{-14} \text{ m}^2/\text{s}$ and $5.7 \times 10^{-16} \text{ m}^2/\text{s}$, respectively²⁰). It was suggested that the slower water diffusion in the Ca-bearing glass is due to binding of H_2O molecules in strong complexes with Ca^{2+} , and to the strengthening of the glass structure by incorporation of divalent cations. It is one of the objectives of this study to get new insights into the

dynamics of hydrous species in silicate glasses and into the effect of different cations on motional processes of H_2O molecules, OH groups and protons.

II. SYNTHESIS AND CHARACTERIZATION OF HYDROUS GLASSES

Hydrous glasses were produced by fusion of glass powder and bidistilled H_2O in an internally heated gas pressure vessel at 1523 K and 500 MPa. The samples we studied are $\text{NaAlSi}_3\text{O}_8 \cdot 0.3\text{H}_2\text{O}$ labeled in this paper as Ab2, $\text{NaAlSi}_3\text{O}_8 \cdot 1.3\text{H}_2\text{O}$ (Ab8), and $\text{Ca}_{0.5}\text{AlSi}_3\text{O}_8 \cdot 1.3\text{H}_2\text{O}$ (AQ8). The labels were derived from the minerals' names albite ($\text{NaAlSi}_3\text{O}_8$) and anorthite/quartz ($\text{CaAl}_2\text{Si}_2\text{O}_8/\text{SiO}_2$). The numbers in the labels denote the H_2O contents in wt. %. A list of the samples and some characteristics are given in Table I. The two water-rich samples contain ≈ 24 mol % (8 wt. %) dissolved H_2O whereas $\text{NaAlSi}_3\text{O}_8 \cdot 0.3\text{H}_2\text{O}$ con-

TABLE I. Sample characterization and IR spectroscopic data. The density of $\text{NaAlSi}_3\text{O}_8 \cdot 0.3\text{H}_2\text{O}$ and $\text{NaAlSi}_3\text{O}_8 \cdot 1.3\text{H}_2\text{O}$ was calculated according to Ref. 21 and the density of $\text{Ca}_{0.5}\text{AlSi}_3\text{O}_8 \cdot 1.3\text{H}_2\text{O}$ was calculated according to Ref. 22. The thickness is an average value for all wafers of the respective composition. Contents of water dissolved as OH and as H_2O were determined from the peak height of the IR absorption bands at 4500 cm^{-1} and 5200 cm^{-1} , respectively. The reported water contents are average values based on 8 to 16 spectra which were recorded on six or more glass plates. The water contents in mol % refer to the composition of oxides, e.g., 9.5 mol% Na_2O –9.5 mol% Al_2O_3 –57 mol% SiO_2 –24 mol% H_2O for Ab8.

Sample	Ab2	Ab8	AQ8	
Anhydrous composition	$\text{NaAlSi}_3\text{O}_8$	$\text{NaAlSi}_3\text{O}_8$	$\text{Ca}_{0.5}\text{AlSi}_3\text{O}_8$	
Hydrous composition	$\text{NaAlSi}_3\text{O}_8 \cdot 0.3\text{H}_2\text{O}$ ($\text{NaAlSi}_3\text{O}_8 + 7 \text{ mol\% H}_2\text{O}$) ($\text{NaAlSi}_3\text{O}_8 + 2 \text{ wt. \% H}_2\text{O}$)	$\text{NaAlSi}_3\text{O}_8 \cdot 1.3\text{H}_2\text{O}$ ($\text{NaAlSi}_3\text{O}_8 + 24 \text{ mol\% H}_2\text{O}$) ($\text{NaAlSi}_3\text{O}_8 + 8 \text{ wt. \% H}_2\text{O}$)	$\text{Ca}_{0.5}\text{AlSi}_3\text{O}_8 \cdot 1.3\text{H}_2\text{O}$ ($\text{Ca}_{0.5}\text{AlSi}_3\text{O}_8 + 24 \text{ mol\% H}_2\text{O}$) ($\text{Ca}_{0.5}\text{AlSi}_3\text{O}_8 + 8 \text{ wt. \% H}_2\text{O}$)	
Density in g/cm^3		2.356	2.274	2.326
Thickness in mm		0.982	0.769	0.775
Water content in mol %		<i>after synthesis</i>		
as OH		4.6±0.1	5.8±0.1	6.3±0.1
as H_2O		2.3±0.2	18.2±0.5	17.8±0.7
total		6.9±0.3	24.0±0.5	24.1±0.7
Water content in mol %		<i>after experiment</i>		
as OH		4.6±0.1	5.8±0.1	6.5±0.1
as H_2O		2.2±0.2	18.0±0.4	17.2±0.3
total		6.8±0.3	23.8±0.4	23.7±0.5

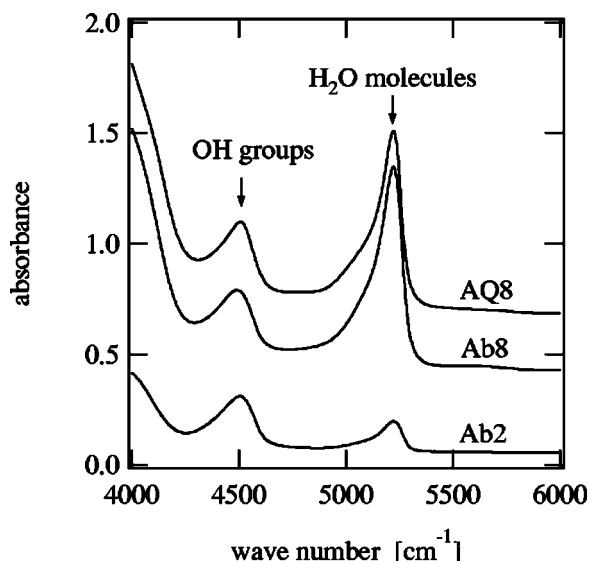


FIG. 2. Near-infrared absorption spectra of $\text{NaAlSi}_3\text{O}_8 \cdot 0.3\text{H}_2\text{O}$ (Ab2), $\text{NaAlSi}_3\text{O}_8 \cdot 1.3\text{H}_2\text{O}$ (Ab8) and $\text{Ca}_{0.5}\text{AlSi}_3\text{O}_8 \cdot 1.3\text{H}_2\text{O}$ (AQ8) recorded after the neutron scattering experiments. The absorbance is normalized to a sample thickness of 1 mm in each case. For clarity, the spectra of Ab8 and AQ8 are plotted with an offset of 0.3 and 0.6, respectively.

tains only 7 mol % (2 wt. %) dissolved H₂O. The water contents given in mol % refer to the composition of oxides. To fill the large area of the sample holder used for neutron scattering six capsules (platinum, size: $30 \times 10 \times 2$ mm³, wall thickness 0.2 mm) were prepared for each composition. All samples for each composition were processed in a single experiment to ensure identical synthesis conditions. Capsules were quenched isobarically with an initial cooling rate of ca. 200 K/min decreasing to ca. 100 K/min in the range of glass transition (between 600 K and 900 K), which depends on water content and anhydrous composition.³

Glass plates were doubly polished and analyzed by IR spectroscopy to determine the concentrations of OH groups and H₂O molecules and to test the homogeneity of hydrous species in the glasses. The wafers were mounted on a hole aperture 2 mm in diameter and spectra were recorded with an FTIR spectrometer Bruker IFS88 using a tungsten light source, a CaF₂ beamsplitter, and an InSb detector. 100 scans were accumulated for each spectrum with a spectral resolution of 4 cm⁻¹. Three to four spectra were recorded on each glass plate before and after the neutron scattering experiments.

Near-infrared absorption spectra of the three glasses are shown in Fig. 2. The bands near 4500 cm⁻¹ and near 5200 cm⁻¹ are attributed to combination modes of OH groups and H₂O molecules, respectively.^{4,10} Concentrations of both species were determined from the peak heights of the bands after subtracting a linear baseline fitted to the 5200 cm⁻¹ band and extended to the 4500 cm⁻¹ band (GG-type baseline²¹). Species concentrations were calculated by Lambert-Beer's law

$$c_i = \frac{A_i}{d \epsilon_i}, \quad (1)$$

where *i* refers to the species OH and H₂O and their corresponding absorption bands at 4500 and 5200 cm⁻¹, respectively. *c_i* is the concentration of water dissolved as species *i*, *A_i* is the absorbance of the combination band related to species *i*, *d* is the sample thickness, and *ε_i* is the molar absorption coefficient. Calibrations of *ε* values and density-water content relationships have been performed earlier, separately for the Na and the Ca glasses.^{8,22}

In the water-rich glasses $\text{NaAlSi}_3\text{O}_8 \cdot 1.3\text{H}_2\text{O}$ and $\text{Ca}_{0.5}\text{AlSi}_3\text{O}_8 \cdot 1.3\text{H}_2\text{O}$ molecular H₂O is the dominant species and only 1/4 of the dissolved water is dissociated to OH groups. In contrast, molecular H₂O is a minor species in $\text{NaAlSi}_3\text{O}_8 \cdot 0.3\text{H}_2\text{O}$ with a relative abundance of only 1/3 (Table I). After the IN10 experiment in which the sample was finally heated to 423 K, the sample of $\text{NaAlSi}_3\text{O}_8 \cdot 1.3\text{H}_2\text{O}$ was pale due to numerous cracks. We attribute the formation of cracks to a spontaneous release of internal stress which is caused by large oversaturation with molecular H₂O (glasses are synthesized at 500 MPa but experiments are performed at ambient pressure). Spontaneous stress release within a few seconds could be observed with a microscope in heating stage experiments with water-rich $\text{NaAlSi}_3\text{O}_8$ glasses (>13 mol % H₂O) but not with water-poor glasses (<13 mol % H₂O). However, the formation of cracks in $\text{NaAlSi}_3\text{O}_8 \cdot 1.3\text{H}_2\text{O}$ is not associated with a loss of water or a change in relative abundance of hydrous species. After the final IN6 experiment all glasses contain unchanged concentrations of OH groups and H₂O molecules (Table I).

III. EXPERIMENTAL SETUP

In this study we used two different spectrometers to perform inelastic neutron scattering, both located at the Institut Laue-Langevin in Grenoble, France.¹⁸ The backscattering spectrometer IN10 has high energy resolution and the time-of-flight spectrometer IN6 gives access to a large energy transfer range. The combination of these two spectrometers allows one to study dynamical processes in a time window of about four decades from 0.2 ps to 2 ns. Corrections of the raw data concerning the background intensity and the detector efficiency were performed using measurements with an empty cell and a vanadium target, respectively. The observed scattering is mainly incoherent from the protons contained in water molecules or OH groups: 79% for the samples containing 24 mol % water ($\text{NaAlSi}_3\text{O}_8 \cdot 1.3\text{H}_2\text{O}$ and $\text{Ca}_{0.5}\text{AlSi}_3\text{O}_8 \cdot 1.3\text{H}_2\text{O}$) but only 52% for $\text{NaAlSi}_3\text{O}_8 \cdot 0.3\text{H}_2\text{O}$.

A. IN10

The backscattering spectrometer IN10 was used with Si-(111) monochromator and analyzer. This corresponds to a neutron wavelength of 6.271 Å and an energy resolution of 0.9 μeV [full width at half maximum (FWHM)]. Energy selection is done via a Doppler monochromator resulting in an accessible energy transfer range from -12 μeV to +12 μeV and thus in an accessible time range from 150 ps to 2 ns. The

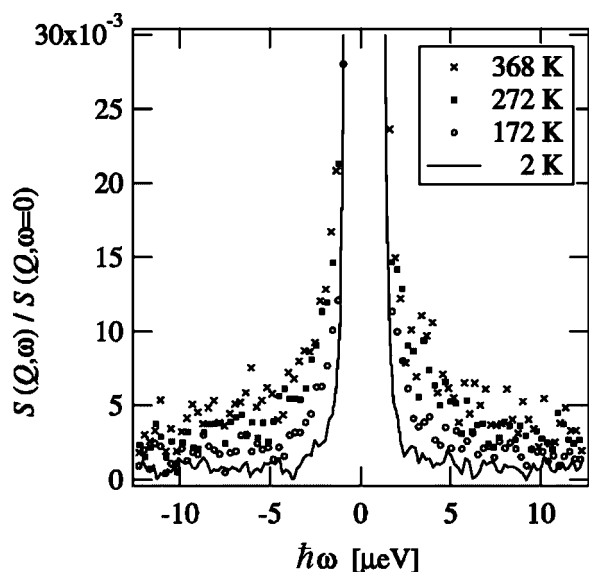


FIG. 3. Normalized neutron backscattering spectra $S(Q, \omega)$ of $\text{NaAlSi}_3\text{O}_8 \cdot 1.3\text{H}_2\text{O}$ (Ab8) obtained on IN10. The data of three detectors with $Q=1.68 \text{ \AA}^{-1}$, 1.85 \AA^{-1} , and 1.96 \AA^{-1} have been averaged to improve the signal-to-noise ratio.

highest scattering angle was 156° corresponding to a maximum momentum transfer of $Q=1.96 \text{ \AA}^{-1}$.

B. IN6

The time-of-flight spectrometer IN6 was used with an incident wavelength of 5.1 \AA resulting in an energy resolution of $100 \mu\text{eV}$ (FWHM) and a momentum transfer range from 0.22 \AA^{-1} to 2.05 \AA^{-1} . At $Q=1.85 \text{ \AA}^{-1}$ the accessible energy transfer range was -1.15 meV to $+15.5 \text{ meV}$ due to the kinematic restriction of neutron energy and momentum. From this a dynamic time window from 0.2 ps to 20 ps results after Fourier transform.

IV. RESULTS

A. IN10

The inelastic spectra for $\text{NaAlSi}_3\text{O}_8 \cdot 1.3\text{H}_2\text{O}$ and $\text{Ca}_{0.5}\text{AlSi}_3\text{O}_8 \cdot 1.3\text{H}_2\text{O}$ measured at the backscattering spectrometer IN10 are shown in Figs. 3 and 4, respectively, for $Q=1.85 \text{ \AA}^{-1}$ and temperatures between 2 K and 370 K . The spectra for all temperatures are scaled to the same maximum intensity. Although there is a clear quasielastic contribution there is only a minor increase of broadening over the large temperature range on an increasing background due to motions which are too fast to be observed on IN10. This appearance indicates a broad distribution of correlation times of which only a few fall into the dynamic window of backscattering spectroscopy. This in turn is probably due to variations in the local environment of water molecules in these amorphous systems.

The inelastic spectra also show differences between $\text{NaAlSi}_3\text{O}_8 \cdot 1.3\text{H}_2\text{O}$ and $\text{Ca}_{0.5}\text{AlSi}_3\text{O}_8 \cdot 1.3\text{H}_2\text{O}$. Whereas the Na glass exhibits a continuous small increase in line broadening towards higher temperatures in the whole temperature

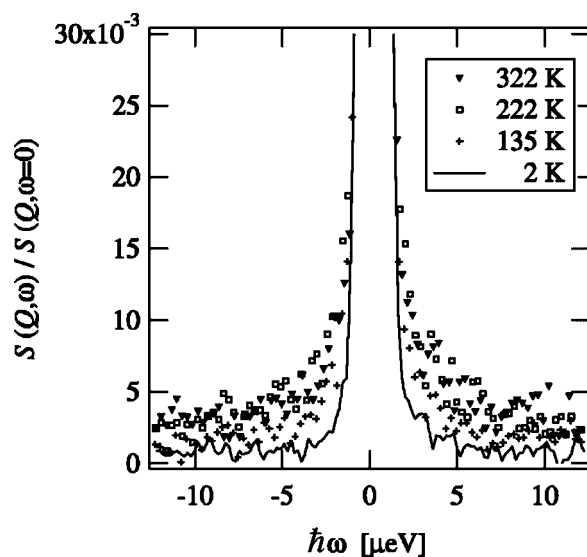


FIG. 4. Normalized neutron backscattering spectra $S(Q, \omega)$ of $\text{Ca}_{0.5}\text{AlSi}_3\text{O}_8 \cdot 1.3\text{H}_2\text{O}$ (AQ8) obtained on IN10. The data of three detectors with $Q=1.68 \text{ \AA}^{-1}$, 1.85 \AA^{-1} , and 1.96 \AA^{-1} have been averaged to improve the signal-to-noise ratio.

range, for the Ca glass the broadening was observed only at temperatures below 250 K (the spectra at 222 K and 322 K almost coincide; see Fig. 4). An explanation might be a narrower distribution of correlation times for the Ca glass. Hence, all dynamic processes become too fast for the time window of IN10 at temperatures above about 250 K while for the Na glass having a broader distribution always a part of the correlation times falls into the time window of this experiment (see also Sec. IV C).

We also performed elastic scans in the temperature range from 2 K to 420 K . The height of the elastic peak is decreasing with increasing temperature due to the onset of fast vibrational motions. This is described by the Debye-Waller factor, from which a mean square displacement $\langle u^2 \rangle$ of the dynamic species (in our experiments protons bound in H_2O molecules or OH groups) can be deduced. The temperature dependence of $\langle u^2 \rangle$ is displayed in Fig. 5 for both water-rich samples. (The time scale of $\langle u^2 \rangle$ follows from the resolution of IN10 to be about 1.4 ns . This is significantly larger than any time scale related to vibrations.) The absence of a pronounced step indicates that there is not a single activated process. At temperatures below about 120 K the Debye-Waller factor increases linearly with temperature indicating that vibrational motions are dominating. At higher temperatures one can see a stronger increase of $\langle u^2 \rangle$ which indicates the onset of further dynamical processes. This transition occurs at lower temperatures for the Ca glass ($\approx 120 \text{ K}$) than for the Na glass ($\approx 150 \text{ K}$). Our findings are consistent with NMR results on silicate glasses indicating the onset of two-fold rotation of H_2O molecules around their bisector axis with correlation times shorter than 10^{-5} s in this temperature range.^{12,13} At temperatures above 250 K the slope of $\langle u^2 \rangle$ vs T decreases again for the Ca glass indicating that the dynamical processes become too fast for the time window of IN10 ($150 \text{ ps} - 2 \text{ ns}$). This contrasts with the data of the Na

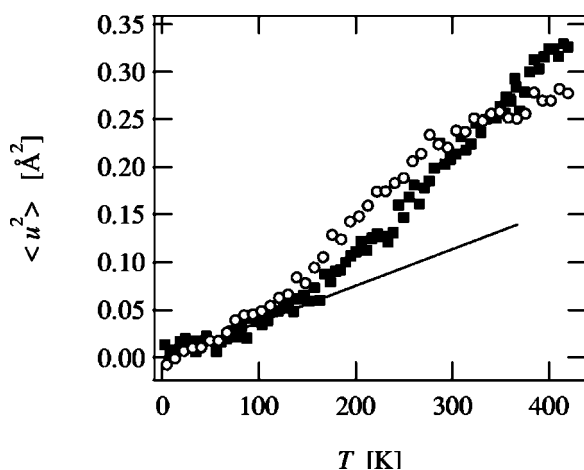


FIG. 5. Mean square displacement $\langle u^2 \rangle$ due to fast motions obtained from elastic scans at IN10 for NaAlSi₃O₈·1.3H₂O (■) and Ca_{0.5}AlSi₃O₈·1.3H₂O (○). The solid line indicates the linear increase of $\langle u^2 \rangle$ at low temperatures.

glass where a significant fraction of the dynamics is visible up to the highest temperatures. These observations are consistent with the results from the inelastic spectra.

B. IN6

The inelastic spectra for NaAlSi₃O₈·1.3H₂O and Ca_{0.5}AlSi₃O₈·1.3H₂O recorded on IN6 are shown in Figs. 6 and 7 for a momentum transfer of 1.85 Å⁻¹ and temperatures between 2 K and 370 K. After scaling the maxima of the elastic peaks to the same height, a continuous quasielastic broadening at the bottom of the peak with increasing temperature is evident. From the spectra at the lowest temperatures also the presence of the glass-specific low energy excitations (boson peak) around 6 meV can be seen. This indicates that the dynamics of the hydrogen, which is the main scatterer in these samples, is not fully decoupled from the dynamics of the glass network.

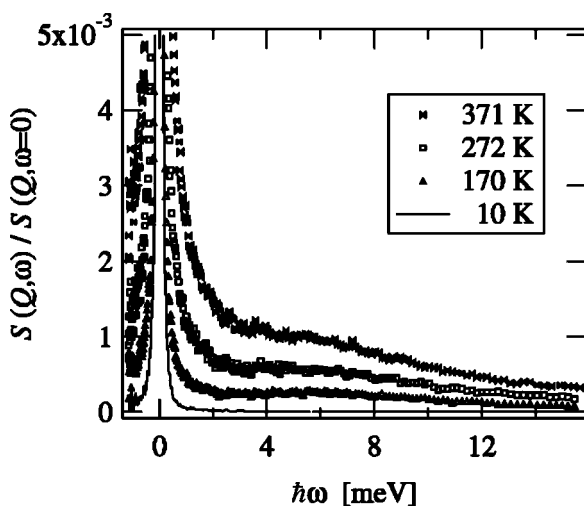


FIG. 6. Normalized neutron time-of-flight spectra $S(Q, \omega)$ of NaAlSi₃O₈·1.3H₂O (Ab8) obtained on IN6. Spectra from different detectors have been interpolated to constant $Q=1.85$ Å⁻¹.

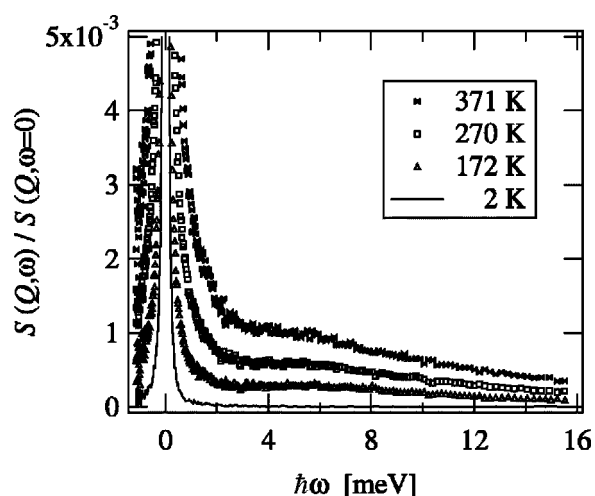


FIG. 7. Normalized neutron time-of-flight spectra $S(Q, \omega)$ of Ca_{0.5}AlSi₃O₈·1.3H₂O (AQ8) obtained on IN6. Spectra from different detectors have been interpolated to constant $Q=1.85$ Å⁻¹.

For comparison inelastic spectra were also recorded for NaAlSi₃O₈·0.3H₂O. In this sample, where the water exists mainly in form of OH groups, the quasielastic broadening of the spectra is much weaker, although much higher temperatures (up to 522 K) were applied. This shows that the broadening in the water-rich glasses is caused mainly by the dynamics of molecular H₂O.

C. Time domain analysis

For a quantitative analysis the inelastic scattering data $S(Q, \omega)$ of both spectrometers were Fourier transformed to the time domain and divided by the corresponding resolution data yielding the intermediate scattering function $S(Q, t)$. The results are shown in Figs. 8 and 9 for both water-rich glasses. The combination of the two spectrometers gives an

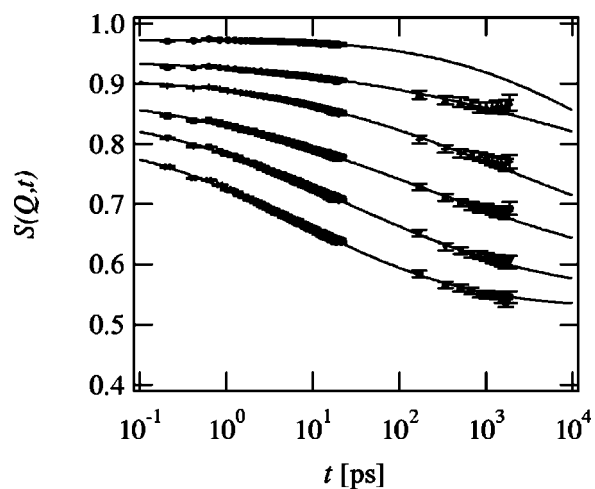


FIG. 8. Incoherent intermediate scattering function $S(Q, t)$ of NaAlSi₃O₈·1.3H₂O (Ab8) calculated by Fourier transform of IN6 data (0.2–20 ps) and IN10 data (150–2000 ps), $Q=1.85$ Å⁻¹. The different curves belong to temperatures of 99 K, 170 K, 221 K, 272 K, 324 K, and 371 K (top to bottom).

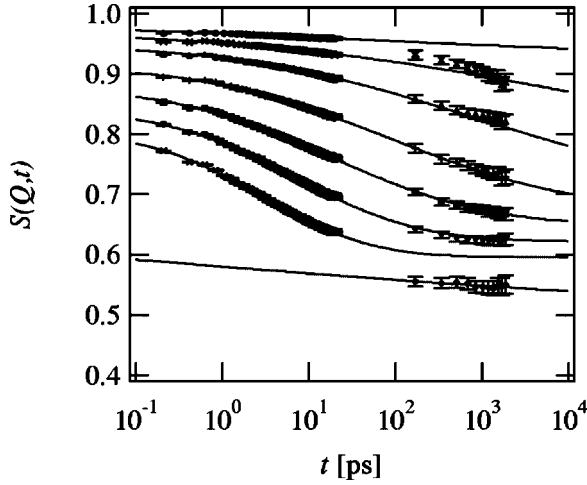


FIG. 9. Incoherent intermediate scattering function $S(Q,t)$ of $\text{Ca}_{0.5}\text{AlSi}_3\text{O}_8 \cdot 1.3\text{H}_2\text{O}$ (AQ8) calculated by Fourier transform of IN6 data (0.2–20 ps) and IN10 data (150–2000 ps), $Q=1.85 \text{ \AA}^{-1}$. The different curves belong to temperatures of 99 K, 134 K, 172 K, 221 K, 270 K, 321 K, 371 K, and 422 K (top to bottom).

overall accessible time range from 0.2 ps to 2 ns, which is 4 decades. The data from the two experiments, namely from the time-of-flight (0.2 ps–20 ps) and the backscattering spectrometer (150 ps–2 ns) fit together rather well without further scaling factors.

The data can be described in the overall time window 0.2 ps–2 ns by comprising the faster processes into a Debye-Waller factor A and those that are effectively “frozen” on that time scale into an elastic incoherent structure factor EISF yielding

$$S(Q,t) = A\{[1 - \text{EISF}]\phi(t) + \text{EISF}\}, \quad (2)$$

where

$$A = \exp(-\langle u_{\text{fast}}^2 \rangle Q^2/3) \quad (3)$$

and

$$\text{EISF} = \exp(-\langle u_{\text{diff}}^2 \rangle Q^2/3) \quad (4)$$

describe the Q dependence of $S(Q,t)$. The function $\phi(t)$ describes the time dependence of $S(Q,t)$ and thus the dynamics of the water in the glasses. To fit the experimental data (solid lines in Figs. 8 and 9) we used a log-normal distribution of correlation times²³

$$g(\ln \tau) = \frac{1}{\sqrt{2\pi}\sigma_{\ln \tau}} \exp\left(-\frac{(\ln \tau - \ln \tau_0)^2}{2\sigma_{\ln \tau}^2}\right) \quad (5)$$

which superimpose to

$$\phi(t) = \int_{\tau=0}^{\infty} \exp(-t/\tau) g(\ln \tau) d \ln \tau. \quad (6)$$

The parameters of the log-normal distribution $g(\ln \tau)$ are the average correlation time τ_0 and the width $\sigma_{\ln \tau}$, both being dependent on temperature. This temperature dependence is used in the next subsection to extract the energy barriers for the observed dynamical process.

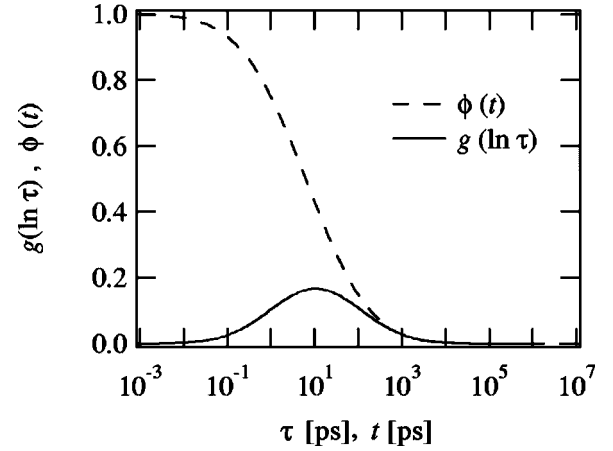


FIG. 10. Log-normal distribution of correlation times $g(\ln \tau)$ and the resulting dynamic function $\phi(t)$ as obtained by fitting Eqs. (2), (6), and (5) to the $S(Q,t)$ data, shown exemplarily for $\text{Ca}_{0.5}\text{AlSi}_3\text{O}_8 \cdot 1.3\text{H}_2\text{O}$ (AQ8) at 321 K, $Q=1.85 \text{ \AA}^{-1}$.

D. Energy barrier model

Since the correlation time τ is expected to show Arrhenius behavior with an activation energy E_A ,

$$\tau = \tau_{\infty} \exp(E_A/k_B T), \quad (7)$$

the log-normal distribution of correlation times corresponds to a normal distribution of activation barriers

$$G(E_A) = \frac{1}{\sqrt{2\pi}\sigma_{E_A}} \exp\left(-\frac{(E_A - E_0)^2}{2\sigma_{E_A}^2}\right), \quad (8)$$

which is reasonable due to the amorphous structure of the glasses. The average activation barrier follows from

$$\tau_0 = \tau_{\infty} \exp(E_0/k_B T). \quad (9)$$

In case that τ_{∞} is constant, i.e., not distributed itself, $\sigma_{\ln \tau}$ and the width of the distribution of activation energies σ_{E_A} are related by

$$\sigma_{\ln \tau} = \frac{\sigma_{E_A}}{k_B T}. \quad (10)$$

The results of fitting Eqs. (2), (5), and (6) to the data are shown as solid lines in Figs. 8 and 9 for $\text{NaAlSi}_3\text{O}_8 \cdot 1.3\text{H}_2\text{O}$ and $\text{Ca}_{0.5}\text{AlSi}_3\text{O}_8 \cdot 1.3\text{H}_2\text{O}$, respectively. To get good results for the fit parameters we had to perform global fits of $S(Q,t)$ keeping EISF constant for all temperatures. We get EISF values of (0.653 ± 0.008) for $\text{NaAlSi}_3\text{O}_8 \cdot 1.3\text{H}_2\text{O}$ and (0.741 ± 0.004) for $\text{Ca}_{0.5}\text{AlSi}_3\text{O}_8 \cdot 1.3\text{H}_2\text{O}$. Figure 10 shows exemplarily the results for the distribution of correlation times $g(\ln \tau)$ and the resulting $\phi(t)$ [Eq. (6)] for $\text{Ca}_{0.5}\text{AlSi}_3\text{O}_8 \cdot 1.3\text{H}_2\text{O}$ at 321 K and $Q=1.85 \text{ \AA}^{-1}$. The average correlation times τ_0 are plotted for both water-rich glasses in Fig. 11 vs inverse temperature. Arrhenius behavior is found over a time range of more than 4 decades. The data are fitted with an exponential function according to Eq. (7) to extract the average activation energy E_0 from the slope and the preexponential factor τ_{∞} from the ordinate intercept. We obtain $E_0 = (0.27 \pm 0.01) \text{ eV}$ for $\text{NaAlSi}_3\text{O}_8 \cdot 1.3\text{H}_2\text{O}$ and E_0

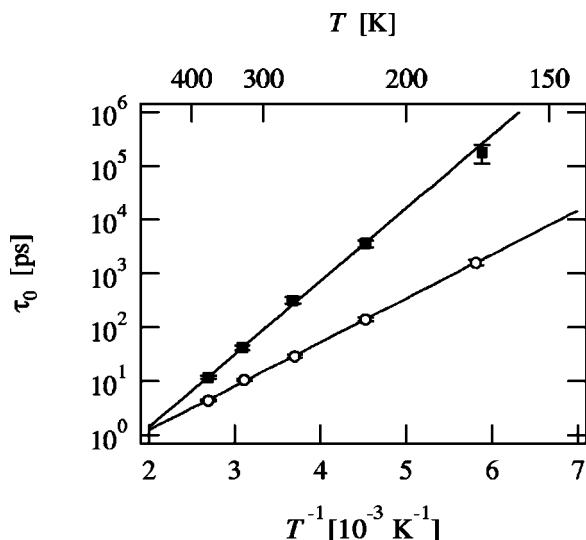


FIG. 11. Average motional correlation times τ_0 obtained from the fit procedure vs inverse temperature for $\text{NaAlSi}_3\text{O}_8 \cdot 1.3\text{H}_2\text{O}$ (■) and $\text{Ca}_{0.5}\text{AlSi}_3\text{O}_8 \cdot 1.3\text{H}_2\text{O}$ (○).

$= (0.16 \pm 0.01)$ eV for $\text{Ca}_{0.5}\text{AlSi}_3\text{O}_8 \cdot 1.3\text{H}_2\text{O}$, i.e., a smaller activation energy for the Ca glass. This is consistent with the results from the elastic scan on IN10 (Fig. 5) where the onset of the dynamic process appears at lower temperatures for $\text{Ca}_{0.5}\text{AlSi}_3\text{O}_8 \cdot 1.3\text{H}_2\text{O}$. The preexponential factor is $\tau_\infty = (2.75 \pm 0.64) \times 10^{-3}$ ps for $\text{NaAlSi}_3\text{O}_8 \cdot 1.3\text{H}_2\text{O}$ and $\tau_\infty = (2.91 \pm 0.32) \times 10^{-2}$ ps for $\text{Ca}_{0.5}\text{AlSi}_3\text{O}_8 \cdot 1.3\text{H}_2\text{O}$. The much smaller τ_∞ value for the Na glass together with the larger activation energy leads to a crossing of both fitting curves at about 500 K (see Fig. 11). At higher temperatures, which are not accessible for our samples, the dynamics would be faster in the Na glass than in the Ca glass. According to Eq. (8), plotting $\sigma_{\ln \tau}$ vs inverse temperature should give a straight line through the origin if τ_∞ is constant. As shown in Fig. 12, the data for both, $\text{NaAlSi}_3\text{O}_8 \cdot 1.3\text{H}_2\text{O}$ and $\text{Ca}_{0.5}\text{AlSi}_3\text{O}_8 \cdot 1.3\text{H}_2\text{O}$, can indeed be rather well described by Eq. (8) (though statistical spread for the Na glass is somewhat larger). The slopes yield $\sigma_{E_A} = (0.107 \pm 0.002)$ eV for $\text{NaAlSi}_3\text{O}_8 \cdot 1.3\text{H}_2\text{O}$ and $\sigma_{E_A} = (0.069 \pm 0.001)$ eV for $\text{Ca}_{0.5}\text{AlSi}_3\text{O}_8 \cdot 1.3\text{H}_2\text{O}$, i.e., the distribution of activation energies is significantly narrower for the Ca glass. This is again in good agreement with the elastic scan on IN10 where the narrow distribution of activation energies and hence correlation times for $\text{Ca}_{0.5}\text{AlSi}_3\text{O}_8 \cdot 1.3\text{H}_2\text{O}$ passes the experimental time window faster than for $\text{NaAlSi}_3\text{O}_8 \cdot 1.3\text{H}_2\text{O}$ where due to the broader distribution always one part of the correlation times falls into the accessible time window. In summary, the results for E_A and σ_{E_A} can be used to plot the distributions of activation energies according to Eq. (8) for both glasses; see Fig. 13.

V. DISCUSSION

A. Comparison of dynamic processes in glasses

Most of the information on the dynamics of hydrous species in silicate glasses was obtained from water diffusion

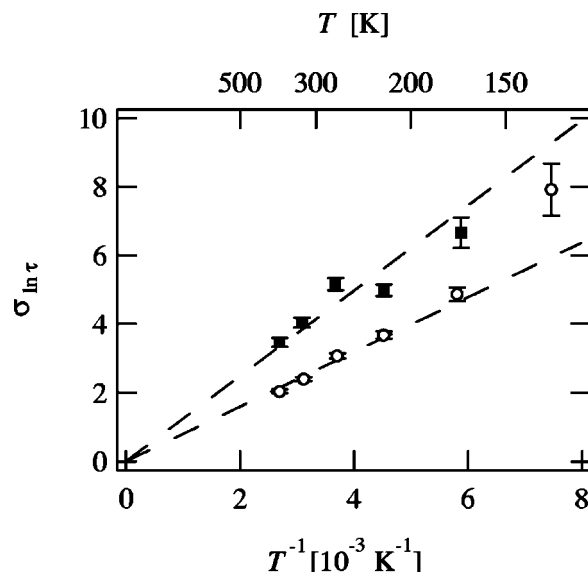


FIG. 12. Width $\sigma_{\ln \tau}$ of the log-normal distribution of motional correlation times vs inverse temperature for $\text{NaAlSi}_3\text{O}_8 \cdot 1.3\text{H}_2\text{O}$ (■) and $\text{Ca}_{0.5}\text{AlSi}_3\text{O}_8 \cdot 1.3\text{H}_2\text{O}$ (○).

studies at elevated temperatures, mainly near and above the glass transition temperature. Other sources of information are IR and NMR spectroscopy and electrical conductivity measurements. The basic results and ideas from these studies are summarized in the following section and compared to our results.

Migration of H₂O molecules has been inferred to be the fundamental mechanism for the transport of water in polymerized glasses and melts.^{24–29} Two mechanisms were proposed to control the diffusion of H₂O molecules. Several authors suggest that H₂O molecules migrate through the silicate network by direct jumps from one cavity to another, and reaction with oxygen of the silicate network results in an immobilization of the H₂O molecules.^{30–32} Another model assumes that the reaction between H₂O molecules and network oxygen forming a pair of OH groups is a transition state during movement of water.^{24,25,28,33} The rate-controlling

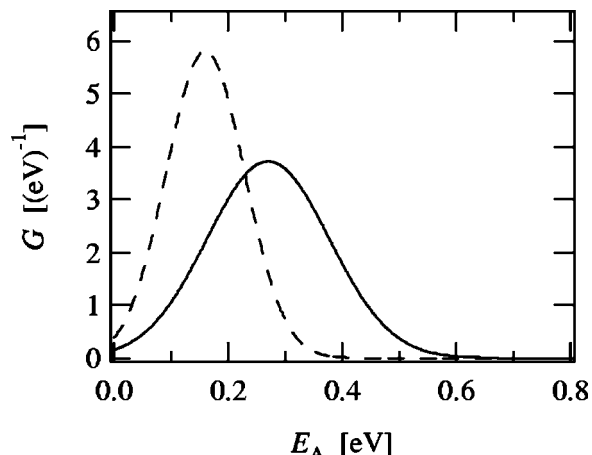


FIG. 13. Normal distribution of activation energies for $\text{NaAlSi}_3\text{O}_8 \cdot 1.3\text{H}_2\text{O}$ (Ab8, solid line) and $\text{Ca}_{0.5}\text{AlSi}_3\text{O}_8 \cdot 1.3\text{H}_2\text{O}$ (AQ8, dashed line).

mechanism may vary with temperature. Above the glass transition, structural relaxation is fast favoring the formation of transient OH group pairs. On the other hand, at low temperatures in the rigid glass structural relaxation is too slow to stabilize the extended transition state required for the formation of OH pairs. Furthermore, at temperatures far below the glass transition the kinetics are too slow to achieve equilibrium for hydrous species. A model for diffusion of water under such nonequilibrium conditions was developed and successfully tested for silica glass by Doremus.³¹

The diffusivity of water is strongly enhanced in aluminosilicate glasses when the alkali content exceeds the quantity required for charge-compensation of aluminium³⁴ implying that nonbridging oxygen can play an important role in the transport of H₂O. Haider and Roberts³⁴ suggested that coupled motion of H⁺ and OH⁻ is a predominant mechanism in depolymerized glasses.

Extrapolated diffusivities of H₂O molecules and protons in silicate glasses are smaller than 10⁻¹⁶ m²/s at temperatures below 400 K,³⁵ corresponding to jump rates smaller than 2 × 10⁻³ s⁻¹ if a jump distance of 5 Å is assumed. This estimate demonstrates that hopping of hydrous species is too slow to contribute to the dynamic effect observed in our neutron scattering experiments. Another support for this interpretation is given by the higher activation energies for water diffusion [0.6–1.0 eV (Refs. 20, 24, 28, 29, 32, and 34)] and proton conduction [0.9 eV (Ref. 35)] compared to the values found in our neutron scattering study.

Evidence for dynamic processes of hydrous species at low temperatures is given only by NMR spectroscopy. A deuterium NMR study using composite-pulse quadrupolar echo pulse sequences on D₂O bearing rhyolitic glass indicates that a twofold rotation of D₂O around its bisector axis at 173 K is faster than 10⁻⁵ s.¹² In static ¹H NMR spectra of hydrous alkali aluminosilicate glasses a well resolved Pake doublet (resulting from the strong homonuclear dipole interaction of the two protons in “immobile” water molecules) was observed only at low temperatures around 140 K.^{11,13,17,36} This implies that any H₂O motion is frozen in the glasses at these conditions. With increasing temperature the Pake doublet transforms more and more into a single line due to the onset of rotation of H₂O molecules. The motional freedom depends on glass composition, in particular on the SiO₂ content. A well resolved Pake doublet could not be observed for very SiO₂ rich compositions even at 140 K implying that H₂O molecules have still some motional freedom.¹⁷

Our neutron scattering data gives access to a more detailed picture of the microscopic processes in water-rich glasses at low temperature because a large temperature range down to 2 K was covered. The results are consistent with the NMR findings that rotation of H₂O molecules in aluminosilicate glasses can be activated at temperatures above 100 K. However, it appears that the motion of H₂O molecules strongly depends on their local environment, as reflected by the broad distribution of activation energies (Fig. 13). Thus the fraction of rotating H₂O molecules continuously in-

creases with temperature and even at the highest temperatures studied a part of the H₂O molecules is probably immobile on the time scale of our experiments.

B. Structural interpretations

The inelastic spectra as well as the elastic scans on IN10 indicate that the dynamic process probed by neutron scattering is faster in the Ca-bearing glass than in the Na-bearing glass. This is confirmed by the results of the time domain analysis which give shorter average correlation times and a smaller average activation energy for Ca_{0.5}AlSi₃O₈·1.3H₂O. However, the larger preexponential factor τ_∞ for Ca_{0.5}AlSi₃O₈·1.3H₂O would lead to an inverted situation at high temperatures. The concentration of low-charged cations (Na⁺ and Ca²⁺) which are located in large cavities in the network is lower by a factor of 2 in the Ca-bearing glasses. Hence, interaction between cations and H₂O molecules may be weaker in Ca_{0.5}AlSi₃O₈·1.3H₂O. This interpretation is supported by the increase in motional freedom of H₂O molecules with increasing silica content along the line NaAlSi₃O₈-SiO₂ observed by ¹H NMR spectroscopy.¹⁷ It should be noted that the dynamic processes detected by neutron scattering are strongly localized, i.e., it is a motion within a cavity of the silicate network. The activation barrier for jumps of water molecules from one cavity to another is much higher in the Ca-bearing glass than in the Na-bearing glass.²⁰ This trend reflects the compaction of the network topology by incorporation of divalent cations.

VI. CONCLUSION

The dynamics of water in hydrous aluminosilicate glasses was investigated by quasielastic neutron scattering in the temperature range from 2 K to 420 K. Combination of a backscattering spectrometer with a time-of-flight spectrometer allowed one to investigate the correlation time range from 0.2 ps to 2 ns. The results of elastic scans as well as the temperature dependence of the inelastic spectra $S(Q, t)$ show that the dynamical processes in the Ca glass with 24 mol % water set in at lower temperatures (≈ 120 K) than in the corresponding Na glass (≈ 150 K). The shape of the scattering function $S(Q, t)$ indicates a distribution of activation barriers for the dynamics of the water due to the disordered structure of the glasses. In the Ca glass the average activation energy (0.16 eV) is smaller than in the Na glass (0.27 eV) and the (normal) distribution of activation barriers is narrower in the Ca glass ($\sigma_{E_A} = 0.07$ eV) than in the Na glass ($\sigma_{E_A} = 0.11$ eV). The dynamical process is attributed to rotational motion of the water molecules. Rotation of H₂O molecules is faster in the Ca-bearing glass than in the Na-bearing glass though their long-range translational motion is slower.

ACKNOWLEDGMENT

We are grateful to the Deutsche Forschungsgemeinschaft for financial support.

*Electronic address: indris@pci.uni-hannover.de

†Electronic address: heitjans@pci.uni-hannover.de; URL: <http://www.unics.uni-hannover.de/pciheitjans/akhei.html>

- ¹K. U. Hess and D. B. Dingwell, *Am. Mineral.* **81**, 1297 (1996).
- ²P. Richey, A. Lejeune, F. Holtz, and J. Roux, *Chem. Geol.* **128**, 195 (1996).
- ³J. Deubener, R. Müller, H. Behrens, and G. Heide, *J. Non-Cryst. Solids* **330**, 268 (2003).
- ⁴E. M. Stolper, *Contrib. Mineral. Petrol.* **81**, 1 (1982).
- ⁵M. C. Johnson, A. T. Anderson, Jr., and M. J. Rutherford, *Rev. Mineral.* **30**, 281 (1994).
- ⁶G. Heide, M. Leschik, and G. H. Frischat, *Geochemistry* **61**, 187 (2001).
- ⁷L. M. Anovitz, J. M. Elam, L. R. Riciputi, and D. R. Cole, *J. Archeol. Sci.* **26**, 735 (1999).
- ⁸H. Behrens, C. Romano, M. Nowak, F. Holtz, and D. B. Dingwell, *Chem. Geol.* **128**, 41 (1996).
- ⁹H. Behrens, M. Meyer, F. Holtz, D. Benne, and M. Nowak, *Chem. Geol.* **174**, 275 (2001).
- ¹⁰H. Scholze, *Naturwissenschaften* **47**, 226 (1960).
- ¹¹R. F. Bartholomew and J. W. H. Schreurs, *J. Non-Cryst. Solids* **38-39**, 679 (1980).
- ¹²H. Eckert, J. P. Yesinowski, E. M. Stolper, T. R. Stanton, and J. Holloway, *J. Non-Cryst. Solids* **93**, 93 (1987).
- ¹³B. C. Schmidt, H. Behrens, T. Riemer, R. Kappes, and R. Dupree, *Chem. Geol.* **174**, 195 (2001).
- ¹⁴L. A. Silver, P. D. Ihinger, and E. M. Stolper, *Contrib. Mineral. Petrol.* **104**, 142 (1990).
- ¹⁵S. Ohlhorst, H. Behrens, and F. Holtz, *Chem. Geol.* **174**, 5 (2001).
- ¹⁶H. Eckert, J. P. Yesinowski, L. A. Silver, and E. M. Stolper, *J. Phys. Chem.* **92**, 2055 (1988).
- ¹⁷B. C. Schmidt, T. Riemer, S. C. Kohn, H. Behrens, and R. Dupree, *Geochim. Cosmochim. Acta* **64**, 513 (1999).
- ¹⁸M. Bée, *Quasielastic Neutron Scattering* (Adam Hilger, Bristol, 1988).
- ¹⁹T. Springer and R. E. Lechner, in *Diffusion in Condensed*

Matter – Methods, Materials, Models, edited by P. Heitjans and J. Kärger (Springer, Berlin, in press).

- ²⁰H. Behrens and F. Schulze, in *Applied Mineralogy in Research, Economy, Technology and Culture*, edited by D. Rammlmair, J. Mederer, Th. Oberthür, R. B. Heimann, and H. Penttinghaus (Balkema, Rotterdam, 2000), p. 95.
- ²¹A. C. Withers and H. Behrens, *Phys. Chem. Miner.* **27**, 119 (1999).
- ²²S. Ohlhorst, H. Behrens, F. Holtz, and B. C. Schmidt, in *Applied Mineralogy in Research, Economy, Technology and Culture*, edited by D. Rammlmair, J. Mederer, Th. Oberthür, R. B. Heimann, and H. Penttinghaus (Balkema, Rotterdam, 2000) p. 193.
- ²³R. Zorn, B. Frick, and L. J. Fetters, *J. Chem. Phys.* **116**, 845 (2002).
- ²⁴G. J. Roberts and J. P. Roberts, *Phys. Chem. Glasses* **7**, 82 (1966).
- ²⁵M. Tomozawa, *J. Am. Ceram. Soc.* **68**, C251 (1985).
- ²⁶G. J. Wasserburg, *J. Geol.* **96**, 363 (1988).
- ²⁷M. Helmich and F. Rauch, *Glastech. Ber.* **66**, 195 (1993).
- ²⁸H. Behrens and M. Nowak, *Contrib. Mineral. Petrol.* **126**, 377 (1997).
- ²⁹Y. Zhang and H. Behrens, *Chem. Geol.* **169**, 243 (2000).
- ³⁰R. H. Doremus, in *Reactivity of Solids*, edited by C. W. Mitchell (Wiley, New York, 1969), p. 667.
- ³¹R. H. Doremus, *J. Mater. Res.* **10**, 2379 (1995).
- ³²Y. Zhang, E. M. Stolper, and G. J. Wasserburg, *Geochim. Cosmochim. Acta* **55**, 441 (1991).
- ³³M. Nowak and H. Behrens, *Contrib. Mineral. Petrol.* **126**, 365 (1997).
- ³⁴Z. Haider and G. J. Roberts, *Glass Technol.* **6**, 158 (1970).
- ³⁵H. Behrens, R. Kappes, and P. Heitjans, *J. Non-Cryst. Solids* **306**, 271 (2002).
- ³⁶V. O. Zavel'sky, N. I. Bezman, and V. A. Zharikov, *J. Non-Cryst. Solids* **224**, 225 (1998).
- ³⁷In the literature often the term “relaxation time” is used. The motional correlation time is of the order of the mean residence time.